Astron. Astrophys. 321, 568–574 (1997)

ASTRONOMY
AND
ASTROPHYSICS

The molecular envelope around T Tauri and the nature of NGC 1555

K.-F. Schuster[1,2,5], **A.I. Harris**[1,3,5], **and A.P.G. Russell**[1,4,5]

[1] Max-Planck-Institut für Extraterrestrische Physik D-85740 Garching, Germany.
[2] Institut de Radio Astronomie Millimetrique, F-38406 St Martin d'Heres Cedex, France
[3] Five College Astronomy Department; and Department of Physics and Astronomy, University of Massachusetts, USA
[4] Royal Observatory, Blackford Hill, Edinburgh EH9 3HJ, UK
[5] Visiting Astronomer at the James Clerk Maxwell Telescope

Received 4 June 1996 / Accepted 10 October 1996

Abstract. We present maps of the ^{12}CO(3–2) and C^{18}O(2–1) emission around T Tauri. By comparison of the two lines measured with similar spatial resolution we are able to discriminate between the different components of molecular circumstellar material and to derive constraints for possible source models. In particular we are able to trace the outflowing molecular components. We propose a multiple outflow system with stellar wind envelope interaction to explain the morphology and dynamics of the ^{12}CO(3–2) and C^{18}O(2–1) emitting gas.

Key words: stars: T Tau – ISM: NGC 1555 – ISM: jets and outflows – radio lines: ISM – stars: pre-main-sequence

1. Introduction

The evolutionary state of classical T Tauri stars is now generally thought to be a transition phase between heavily embedded sources and pre-main sequence stars with little circumstellar material. Due to superposition of radiation from different components of the circumstellar matter such as outflows, envelopes and circumstellar disks, the geometry of these objects is quite often difficult to disentangle and may lead to contradictory conclusions. Circumstellar material and young stars form complex systems with mutual interactions in form of radiation, shocks, mass loss, infall and accretion.

To study these phenomena we used ^{12}CO(3–2) and C^{18}O(2–1) observations in the well known prototypical young low mass stellar object T Tauri to investigate the molecular gas with low and moderately high temperatures. While the C^{18}O(2–1) observations yield estimates of column densities, the ^{12}CO(3–2) emission can be used to search for warm gas. Because the radiation field on the scale size of our spatial resolution (12″-14″$\sim$ 2000 AU at 140pc) is weak in regions of low mass star formation, the warm gas is an indicator of shocks between fast moving components and quiescent envelope material (Schuster et al. 1993 and 1994)

Outflows have been detected in T Tauri with many different tracers in the optical and radio regions. Optical jets have been reported by Bührke et al. 1986, Böhm & Solf 1994, van Langefelde et al. 1994[a] and Robberto et al. 1995. The molecular outflows in T Tauri have been observed by Edwards & Snell 1982, Levrault 1988, Schuster et al. 1993 and Momose et al. 1996. H_2O Maser emission probably coming from interaction of outflowing gas with dense parts of the envelope was first detected by Knapp and Morris 1976 and confirmed by several other groups. A tentative detection of outflowing neutral atomic gas was reported by Ruiz et al. 1992. A circumstellar disk was proposed for T Tauri by Weintraub et al. 1988. Detection of infall was claimed by van Langefelde et al. 1994[b].

Furthermore T Tauri is a binary system with a visible component (T-Tau N) and a more embedded object (T-Tau S) with an angular separation of 0.7″. Discussions of the stellar system can be found in Skinner & Brown 1994 and Ghez et al. 1991. Ghez et al. 1991 found a strong variability for T-Tau S in the IR. One of the main questions remains the nature of the envelope material on scale sizes of several 1000 AU's. In this paper we will discuss the different possible geometries and mechanisms on this scale size in the light of our observations.

2. Observations

The CO(3–2) observations presented here were taken at the JCMT in 1991 December. Additional C^{18}O(2–1) observations were performed at the IRAM 30m telescope in 1994 January. The overall observation time for the CO(3–2) maps around T Tauri was about 15 hours. The CO(3–2) observations were performed with the JCMT facility SIS mixer receiver at 345 GHz. This single channel receiver had a DSB noise temperature of $\sim$180 K. The beam was 14.3″$\pm$0.2″ and the main beam efficiency η_{mb} was 0.56$\pm$0.02. The backend was an acousto optical

spectrometer with a resolution of 0.25 MHz (0.22 km s^{-1}). The observations were made in beam-switching mode with an off position 1200″ in azimuth with regular check for emission in the off position. We integrated on the center position after every 6 to 8 mapping positions to check pointing and calibration. The map of T Tauri contains 108 spectra with a 15″ spacing with a central area of $\pm 15 \times \pm 30''$ at half beam sampling. From typical variations of the central position line flux observed on different nights and by taking typical values for the system calibration accuracy into account we estimate the absolute calibration accuracy to be 20-30% and the relative calibration accuracy better than 20%.

The C^{18}O(2–1) map was made at the IRAM 30m telescope. This map covers about the same field as the CO(3–2) map obtained from the JCMT. The beam of the 30m telescope is 12″ for CO(2–1) transitions, nearly the same as the CO(3–2) beam at the JCMT. The map contains 76 points on a 15″ grid where the inner region of ±15″ was sampled with a diagonal interleaving, resulting in a 10.6″ spacing.

The C^{18}O(2–1) observations were made by frequency switching over ±15 MHz with a 4 second period; this interval was chosen to minimize baseline ripples due to standing waves (see Thum et al. 1995). The backend was an autocorrelator with a frequency resolution of 39 kHz resulting in a velocity resolution of 0.05 km s^{-1} per channel for the C^{18}O(2–1) transition. With this high resolution it was possible to study the dynamics of the quiescent gas of the outer part of the object's envelope. We checked calibration and pointing by frequent integrations on the central position. The relative calibration accuracy in the scans taken on the central position was better than 10% .

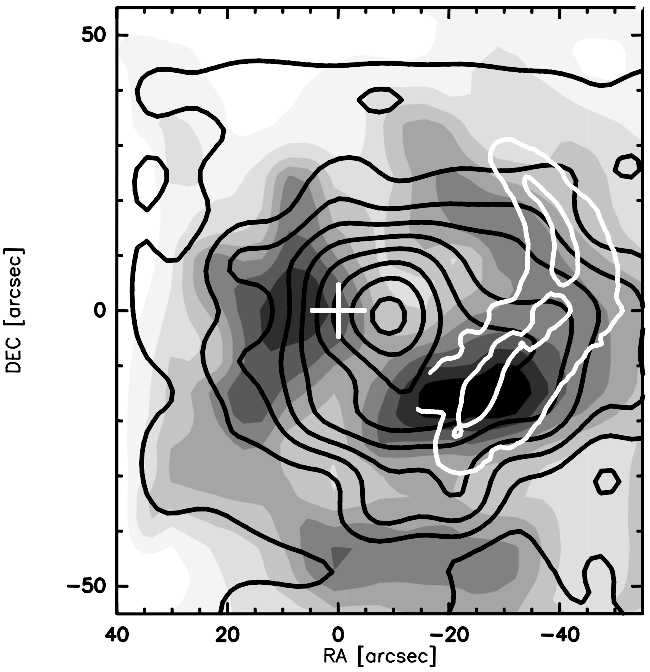

Fig. 1. C^{18}O(2–1) (grey scale) and ^{12}CO(3–2) emission (black contours) near T-Tauri, with 12″ and 14″ resolution respectively. Contours for C^{18}O(2–1) start at 0.46 K km s^{-1} with 0.23 K km s^{-1} steps. Contours for ^{12}CO(2–1) start at 20 K km s^{-1} with 15 K km s^{-1} steps. The cross marks the position of T Tauri (α(2000) = 04^{h}19^{m}04^{s}, δ(2000) = 19°25′05″) . The white contours indicate the intensity of the reflected light in K band (Hodapp 1994); the contours around the star have been omitted.

3. Results

Fig. 1 shows the integrated line intensities of ^{12}CO(3–2) and C^{18}O(2–1) superposed on the lowest contours of the K band emission (Hodapp 1994). All results in the following are given on a T_{mb} scale.

3.1. CO(3–2) *emission*

The CO(3–2) emission shows a pronounced maximum about 10″ west of T Tauri. A similar offset was already found in observations of the CO(6–5) transition (Schuster et al. 1993). From the CO(6–5) observations, a kinetic temperature of > 80 K was derived for the gas within 15″ around the star. The CO(3–2) emission extends to the reflection nebula NGC 1555. In other directions the emission drops off within about 20″ of T Tauri. The rest of the map shows some background emission which is probably due to colder diffuse material. By comparison with the results from Schuster et al. 1993 we estimate the total mass of warm gas (> 60 K) to be $2 - 5 \cdot 10^{-2}\ M_{\odot}$. If this material were distributed homogeneously on a scale of $\sim 2000 - 5000$ AU (corresponding to the 15″-40″emission region west of T Tauri) it would stop visible light from the star from reaching NGC 1555. As this is not the case, and as the light illuminates the reflection nebula with a large angle, the material traced with the CO(3–2) line is probably located in the back- or foreground.

Fig. 2 shows the CO(3–2) channel maps. Most of the emission is at the line center between 7 and 9 km s^{-1}. The blueshift of the emission increases with distance from T Tauri along a bow-shaped ridge toward NGC 1555. This indicates that NGC 1555 is not a separate molecular cloud but forms the front of a cavity-like structure west of T Tauri. The red shifted emission is less structured. The maximum of this emission is slightly north of T Tauri, and expands with an elliptical shape towards NGC 1555. While the emission near T Tauri is at 8 km s^{-1}, close to the systemic velocity, the CO(3–2) emission at NGC 1555 has high velocity components offset to the blue by up to 9 km s^{-1} (-1 to 0 km s^{-1} V_{LSR}). These high velocity components are not very massive but are important signatures of the dynamics of the envelope. For the redshifted emission we find no significant variation of position with velocity. We do not detect a redshifted lobe east of T Tauri. This mass loss asymmetry around T Tauri is also found in optical forbidden line transitions (Böhm & Solf 1994).

3.2. C^{18}O(2–1) *emission*

The C^{18}O(2–1) integrated line emission is shown in grey scale in Fig. 1, and reveals a well defined envelope with a diame-

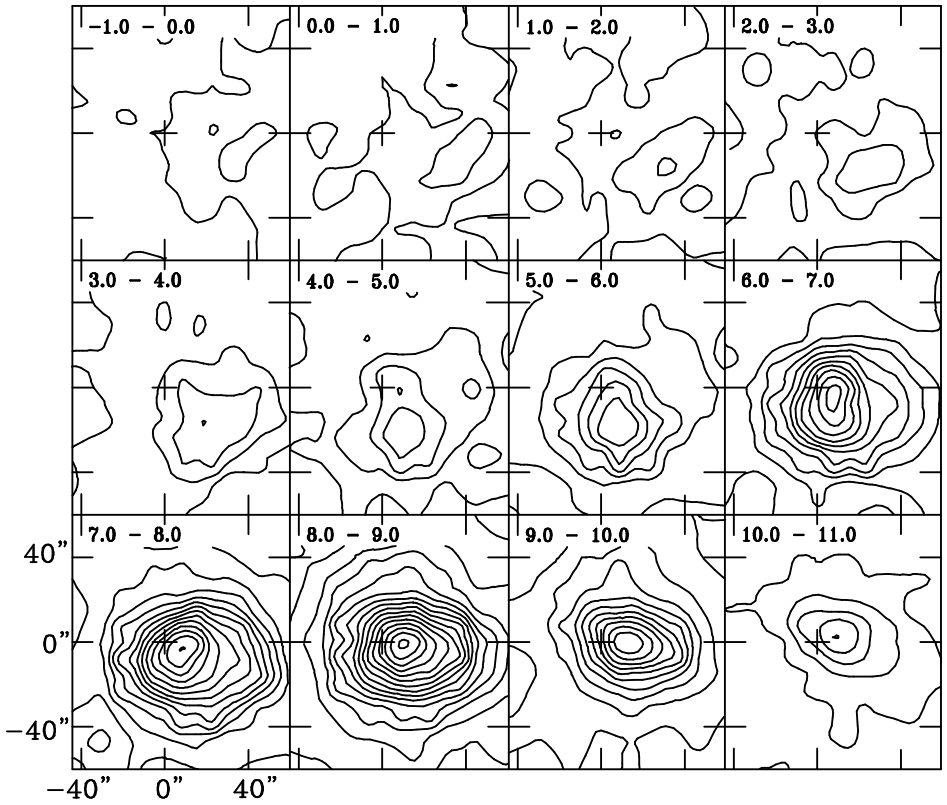

Fig. 2. Channel maps of the ^{12}CO(3–2) emission between -1 and +11 km s^{-1} in 1.0 km s^{-1} intervals. The lowest contour corresponds to an intensity of 2.1 K km s^{-1} with equidistant spacing of 2.1 K km s^{-1} for all following contours. LSR velocities (km s^{-1}) are indicated in the top left of each box. The angular scale is indicated in arcsec at the lower left box, the cross marks the position of T Tauri.

ter of about 1.5′. While the extent is the same as that of the CO(3–2) emission, the detailed morphology is quite different. The C^{18}O(2–1) emission shows a clear shell geometry extending to the west. This shell is closely correlated with the reflected IR emission in K band. Almost the entire reflection nebula NGC 1555 can be traced in C^{18}O(2–1). Only at the end of the nebula lying to the north-west of T Tauri is there a displacement between the C^{18}O(2–1) and the reflected light. However, the morphology of the reflection nebula arises not only from the distribution of the scattering material but also from the illumination pattern, which can deviate considerably from that of a point source if circumstellar material blocks part of the light. The shell is not homogeneous but has a strong maximum 30″ south-west of T Tauri. Another maximum is at 10″ east of T Tauri. The material connected to the second maximum is likely to be responsible for the slight asymmetry of the NIR pattern around the star.

It is interesting that the center of mass of the envelope emission does not coincide with the star but is about 15″ south-west. The C^{18}O(2–1) shows an extra rim at the very south of our map which together with the maximum east of T Tauri forms a spiral-like structure.

With an C^{18}O to H$_2$ abundance ratio of $\sim 1.7 \cdot 10^{-7}$ we derive a total mass of $0.3 M_{\odot}$ for the envelope (for gas temperatures around 20 K). It is important to note that this mass is high enough that long wavelength measurements from IRAS or ISO with low spatial resolution are heavily blended by this envelope material and do not reflect close circumstellar or circumbinary material only ! The maximum intensity found at the clump south-west of T Tauri is 2.25 K km s^{-1} which implies a H$_2$ column density of $8 \cdot 10^{21}$ cm^{-2} or an A$_v$ of 8.6 mag. The maximum 10″ east of T Tauri corresponds to 2 K km s^{-1} or $N_{H_2} = 7 \cdot 10^{21}$ cm^{-2}. For the rim at the position of NGC 1555 we derive $N_{H_2} = 5 \cdot 10^{21}$ cm^{-2}. We conclude that unless there is very strong clumping on scale sizes $< 10''$ (which should be visible in scattered light and is therefor unlikely except for the immediate stellar vicinity) the emission is optically thin over the whole envelope.

It is surprising that there is no maximum at the star itself. However with 12″ resolution we will certainly miss any compact circumstellar or circumbinary disk for reasons of beam filling. On the scale of our resolution we derive a H$_2$ column density of $5.9 \cdot 10^{21}$ cm^{-2} or an A$_v$ of 6.4 mag towards the star itself. This compares to an A$_v$ of 4.2 mag towards T Tauri S and an A$_v$ of 1.5 mag towards T Tauri N, values which were adopted by Ghez et al. 1991. The fact that we find a large scale column density corresponding to a higher visual extinction than actually found by optical observations means that either the stellar system is in front of the detected material or the star is seen through a hole in a foreground layer with a hole size considerably smaller than the radio beam.

For all reasonable geometries we conclude from the derived column densities that the K band absorption and scattering depths of NGC 1555 are < 0.5 in all directions (for K band scattering cross-sections from Draine & Lee 1984). In other words, both the scattered NIR light and the C^{18}O(2–1) emission trace column density. This is the reason for the good correlation between the two observations.

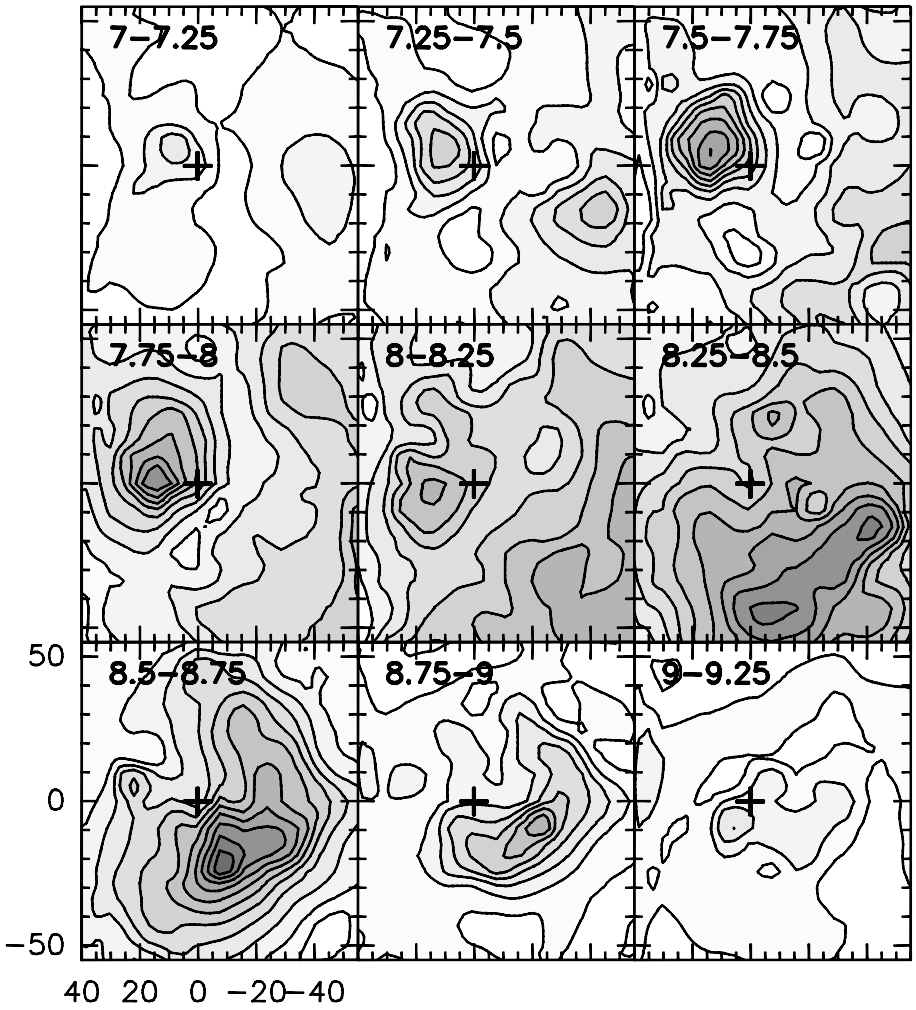

Fig. 3. Channel maps of the $C^{18}O$(2-1) emission between 7 and 9.25 km s^{-1} in 0.25 km s^{-1} intervals. The lowest contour (separation white to grey) corresponds to an intensity of 0.05 K km s^{-1} with equidistant spacing of 0.05 K km s^{-1} for all following contours. LSR velocities (km s^{-1}) are indicated in the top left of each box. The angular scale is indicated in arcsec at the lower left box, the cross marks the position of T Tauri.

The channel maps of the $C^{18}O$(2–1) emission are given in Fig. 3. The dominant structure revealed by these channel maps is the velocity structure shifting from a compact blue region northeast of the star at a velocity of $7-8$ km s^{-1} to a compact red emission southwest of the star at velocities > 9 km s^{-1}. The emission at velocities between these extremes is distributed in a much more complex manner. There seems to be another faint blue component at the outer edge of NGC 1555. This component is probably connected to the blueshifted high velocity gas measured in CO(3–2). At velocities between 8.25 and 9 km s^{-1} the emission forms an extended half-shell $\sim 20''-40''$ west and southwest of T Tauri which reproduces well the pattern of NGC 1555 for velocities between 8.5 and 9 km s^{-1}. For velocities around 8.5 km s^{-1} there is also an indication of a faint compact emission $10''-15''$ east of T Tauri. Altogether there are four emission regions with clear velocity shift in respect to the systemic velocity. These blue and redshifted regions are arranged in an antisymmetric pattern as outlined in Fig. 4 . Momose et al. 1996 found a similar pattern in ^{13}CO(1–0) interferometric measurements with a higher angular resolution. As this velocity structure seems to be a key issue in the picture of the envelope around T Tauri we will discuss different models in the next section.

The mean velocity of the envelope is $8-8.25$ km s^{-1} which corresponds to the spectral absorption feature found by van Langefeld et al. 1994[b] in interferometric HCO^+(1–0) observations. They proposed a homogeneous large scale foreground layer of cold gas which absorbs radiation from warmer redshifted infalling gas. However at the position of T Tauri, the $C^{18}O$(2–1) emission shows a relatively big hole ($10''$-$15''$) at velocities around 8.25 km s^{-1}. Such a pattern supports more a real depletion of $C^{18}O$ than infall at this position. The peak velocity of $7.5-8$ km s^{-1} which is seen in higher transitions towards the stellar position is probably due to the blue maximum to the east of the star.

4. Discussion

How can the significant difference between the CO(3–2) and the $C^{18}O$(2–1) emission be explained ? For the outer regions of the envelope the most important factors are likely to be the difference in excitation temperature (16 K above ground for J = 2 vs. 32 K for J = 3) and the very different optical depths due to

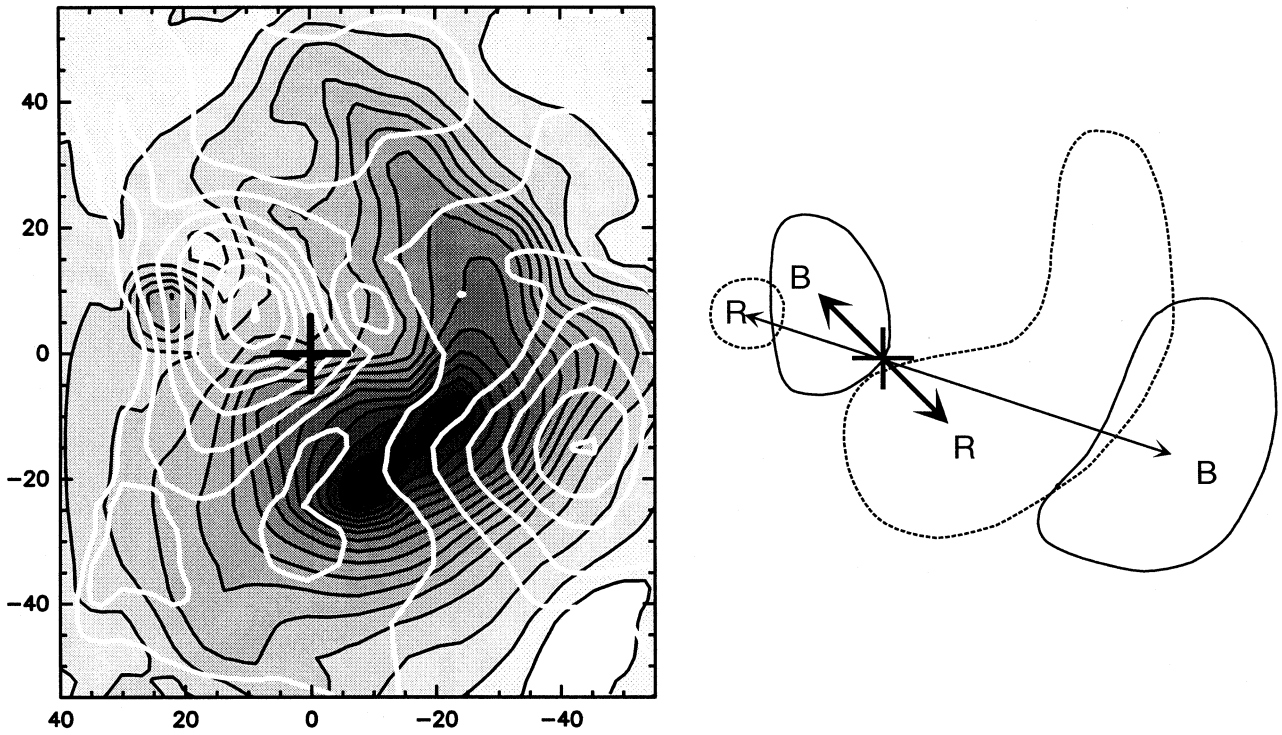

Fig. 4. left: Overlay of red and blueshifted $C^{18}O$(2-1) emission. The redshifted emission between 8.5 and 9 km s^{-1} is given in a grey scale plot while the blue emission between 7 and 7.5 km s^{-1} is plotted with white contours. Angular scales and contour spacings are like in Fig. 3. right: Sketch of the proposed multiple outflow system.

the difference in abundance. In such regions the radiation energy input from the star is low and we probably see CO(3–2) emission from fast moving shock excited gas while the $C^{18}O$(2–1) reflects cooler and more quiescent material.

In particular, for the close region around T Tauri where CO(3–2) peaks, it is possible that in addition to dynamical heating effects we see deviations from the nominal abundance ratio of the two isotopic molecules. Near the star, selective destruction of $C^{18}O$ due to stellar UV light can occur while ^{12}CO is more self-shielded. Such processes can be very efficient (see Warin et al. 1995) on H_2 column density scales of $10^{21} - 10^{22}$ cm^{-2}, close to those found in our observations. To study such mechanisms further investigations, in particular of the true UV flux around T Tauri, are necessary.

An important question is whether the detected material is gravitationally bound and part of an infalling envelope or a circumstellar disk or whether the material belongs to an outflow. From ^{12}CO(1–0) interferometric observations Weintraub et al. 1988 claimed a large gaseous disk with the main velocity gradient along a position angle of 45°. Our $C^{18}O$(2–1) measurements reproduce the velocity gradient which led to this interpretation. However there is nothing which could be really identified with a typical circumstellar disk. From the fact that we find the CO(3–2) emission tracing clearly gravitationally unbound material surrounded by the shell of $C^{18}O$(2–1) emission we rather conclude that most of detected material belongs to a general expanding structure. Because of possible projectional effects it is difficult to derive such a conclusion from the $C^{18}O$(2–1) emission alone.

4.1. The velocity pattern and possible geometries

Momose et al. 1996 first recognized that the enigmatic velocity distribution of molecular gas in T Tauri's envelope required an explanation more complicated than a simple bipolar molecular outflow in the plane of sky. Their interferometric ^{13}CO(1–0) observations led them to a single bipolar outflow model with two hollow outflow cones seen nearly pole-on. They further propose that NGC 1555 is identical to the limb of one of this pole-on lobes. By an appropriate combination of inclination angle and outflow opening angle they are able to reproduce at least parts of the observed velocity structure. This model fits well with the fact that optical measurements of T Tauri N imply a pole-on geometry (Herbst et al. 1986). However we find in our data that there are some important points which do not support such a geometry for the envelope itself. Firstly, neither our $C^{18}O$(2–1) nor the Nobeyama ^{13}CO(1–0) data show a clear signature of complete uniform cones but rather is a long north-south gap running about 10″ west from T Tauri. This gap is particularly obvious for the blue shifted $C^{18}O$(2–1) emission between 7 and 8 km s^{-1} and is difficult to explain in the Momose picture.

Secondly and more important, any picture of a cone which is relatively homogeneous (also in outflow direction towards the observer) has severe difficulties in explaining the structure of NGC 1555. We will outline this in the following:

The bright rim measured in $C^{18}O(2–1)$ and the scattered light for NGC 1555 can only either result from limb brightening of a hollow shell or a curved, one-dimensional filament. Here we try to give some arguments for the geometry of NGC 1555 derived from the relation between $C^{18}O(2–1)$ distribution and the K band scattering pattern.

In a simplified picture the intensity of the scattered light is a function of mainly two parameters, with the assumption of a uniform source radiation, isotropic scattering and scattering and absorption optical depths < 1 (Witt 1985). Those parameters are the distance between the scattering material and the source, and the column density of the scattering material along the line of sight. For shells under uniform illumination from a point source this means that limb brightening effects compete with illumination effects due to varying distances between source and scattering material. In other words, in order to get a local maximum in scattered light (as observed in the case of NGC 1555) at a certain offset position from the star, the limb brightening factor has to increase faster with the angular offset than the illumination factor decreases due to the growing distance between light source and scattering material.

It is clear from the given geometry that a pole-on cone without any curvature or longitudinal inhomogeneities (Fig. 5a) cannot produce the observed pattern because no limb brightening or any other zone of increased scattering exists. In addition, any scattered light from material displaced along the line of sight will be much fainter because the distance between source and the scattering material will rapidly increase.

Even for curved shells (Fig. 5b) with a limb brightened rim it is difficult to achieve a local maximum of scattered light. This is because for most of such geometries the true distance between the light source and the scattering material increases very fast. For T Tauri, we find, for an inclination angle of the outflow axis of $10° - 20°$, that the illumination of material at the position of NGC 1555 is about ten times weaker than for the case of an plane-of-sky lobe. This number compares with the typical limb brightening contrast which is a function of tangential radius of the shell and the shell thickness. For reasonable geometries this factor is only about 3-6 for NGC 1555. Our $C^{18}O(2–1)$ measurements imply a factor which is even less, namely about 2-3.

We conclude therefore that if NGC 1555 is part of a hollow outflow cone, then this cone must be near the plane of the sky rather than pole-on (Fig. 5c). Only in such an orientation is the distance for the star to the shell sufficiently constant to reveal the measured limb brightening not only in molecular lines but also in scattered light. If such an outflow lobe is only partially closed (as indicated in Fig. 5c) such a geometry does fit to some extent to the velocity structure because it is possible to find redshifted emission near the star (hatched area) while the blue shifted gas is more advanced. However it is not clear why a similar incompleteness of the lobe should also exist for the outflow east of T Tauri where we find the same velocity pattern on a smaller scale.

A quite different interpretation of the velocity pattern is possible by considering that actually both binary components of T

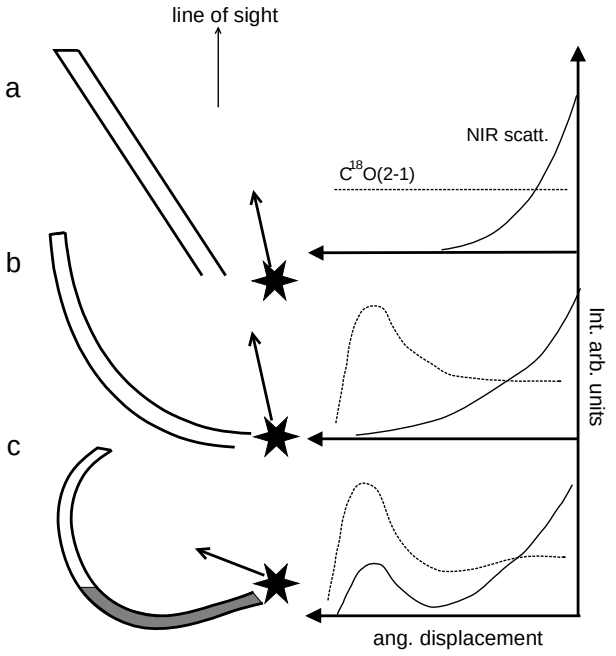

Fig. 5a–c. Different geometries for hollow outflow lobes with uniform shell thickness and the corresponding intensities in $C^{18}O(2–1)$ and scattered NIR light in the optically thin case. **a** conical, open, pole-on outflow lobe, **b** open, convex, pole-on lobe, **c** convex, near-plane-of-sky lobe. The outflow directions are indicated. A Gaussian density distribution across the shell was assumed with the same FWHM thickness for all geometries, beam filling effects were not taken into account. Only geometry c) shows the observed limb brightening in $C^{18}O(2–1)$ **and** scattered NIR light.

Tauri are in an early evolutionary stage and that stellar or disk winds can very well originate from both objects. Böhm and Solf 1994 indeed found with speckle slit spectroscopy that multiple ionized wind components emerge from the binary system in different directions. Such multiple stellar winds certainly leave their fingerprints on the large scale molecular envelope and the velocity structure could very well reflect two different molecular flows driven by the stellar winds with major axes tilted against each other (see Fig. 4, right). In this case there is one bipolar outflow with a position angle of roughly 72° with the blue lobe west of T Tauri very likely driven by the stellar wind which is also responsible for the blue jet found by Bührke et al. 1986. Böhm and Solf 1994 found that this wind is likely originating from T-Tau N. The second flow system would be more compact with a position angle of 45°. NGC 1555 forms the perimeter of the somewhat ill defined redshifted lobe of this flow system. It should be noted however that although the connection between a multiple wind system and a multiple molecular outflow is rather straightforward it is difficult to make a more detailed comparison because the dynamical timescales of molecular flows and ionized stellar winds are generally quite different.

None of the discussed geometries is completely satisfactory but with the existing data we can definitely exclude a large circumbinary disk or a hollow pole-on outflow cone. We be-

Table 1. Mass loss rates derived with different tracers.

$\dot{M}$ [$M_\odot$/y]	Tracer	Reference
$9 \cdot 10^{-7}$	Radio continuum	Schwartz et al. (85)
$3 \cdot 10^{-7}$	HI	Ruiz et al. (92)
$9 \cdot 10^{-10}(Jet)$	[SII],[OI],[NII]	Bührke et al. (86)
10^{-7}–10^{-6}	CO(3–2)	Schuster (94)
$> 3 \cdot 10^{-6}$	$C^{18}O$(2–1)	this work

lieve that the multiple outflow scenario is the most promising to explain the velocity pattern of molecular gas around T Tauri. Our spatial resolution is not high enough to investigate possible effects due to binary rotation or precession although such processes may well pay an important role in the morphology of T Tauri's envelope (see van Langefelde et al. 1994[a] and Schwarz 1990).

4.2. Outflow dynamics

Apart from the fact that the cold slow gas forms a shell structure around the faster warm outflowing material other arguments can be employed to show that a large fraction of the gas traced in $C^{18}O$(2–1) line is gravitationally unbound and probably swept-up material. From the analysis of the scattering pattern of NGC 1555 it could be seen that the main flow axis is likely inclined by more than 45° in respect to the line of sight. For centrally symmetric motions it follows that the velocity of this material is at least $1.4 \cdot v_r$ where v_r is the measured radial velocity relative to the systemic velocity. For a central mass of $3M_\odot$ and a distance of 140pc this means that gas with $|v_r > 0.5\ \mathrm{km\,s^{-1}}|$ outside a radius of 9″ from the star is unbound. We find gas with a total mass of about $0.1M_\odot$ which fulfills these conditions. With $\tau_{dyn} = x/(v_r \cdot \tan(\beta))$ the dynamical timescale is $< 5 \cdot 10^4$ years (where x is the projected distance between shell and star and β the inclination angle of the flow). The derived mass-loss rate is higher than what is derived with other tracers (see Table 1). Unless therefore the gas was ejected in an earlier eruptive event, the movement of the shell is due to deposition of momentum from higher velocity gas into the shell over a longer timescale.

5. Conclusion

Our observations show that T-Tau has a spatially well defined molecular envelope with a total mass of $0.3M_\odot$ and a diameter of 10^4 AU. The internal velocity structure is complex and cannot be explained by a large circumbinary disk or a single bipolar outflow. The comparison between CO(3–2) and $C^{18}O$(2–1) emission shows a cold slow moving rim or shell which can be identified with the reflection nebula NGC 1555 surrounding warmer material traced by our submillimeter observations. The geometry of the reflection nebula makes it likely that the scattering material has an angle close to 90° with respect to the line of sight towards the star. Within the discussed source models we favor a multiple outflow system probably originating from the different components of the binary.

Acknowledgements. We are grateful to D. Downes for help with the manuscript and to R. Genzel for his support. We thank M. Momose for fruitful discussions and our anonymous referee for valuable comments. The JCMT is operated by the Royal Observatory Edinburgh on behalf of Science and Engineering Research Council of the United Kingdom, the Netherlands Organization for Scientific Research, and the National Research Council of Canada.

References

Böhm, K.H. and Solf, J., 1994, ApJ 430, 277.
Bohlin , R.C., Savage, B.D. and Drake, J.F., 1978, ApJ 224, 132.
Bührke, T., Brugel, F.W. and Mundt, R., 1986, A&A 163, 83.
Draine, B.T. and Lee, H.M., 1984, ApJ 285, 89.
Edwards, S. and Snell, R.L., 1982, ApJ 261, 151.
Ghez, A.M., Neugebauer, P.W., Gorham, C.A. et al. 1991, AJ 102 (6), 2066.
Herbst, W., Booth, J.F., Chugainov, P.F. et al. 1986, ApJ 310 L71.
Hodapp, K.W., 1994, ApJS 94, 615.
Knapp, G.R., Morris, M., 1976, ApJ 206, 713.
Lada, C.J., 1987 in I.A.U. Symp. No. 115: Star Forming Regions, eds. M. Peimbert and J. Jugaku, (Dordrecht: Reidel), 1.
Levrault R.M., 1988, ApJS, 67, 289.
Momose, M., Ohashi, N., Kawabe, R., et al. 1996, to appear in ApJ 470.
Robberto, M., Clampin, M., Ligori, S. et al. H.J., 1995, A&A 296, 431.
Ruiz, A., Alonso, J.L. and Mirabel, I.F., 1992, ApJ 394, L57.
Schuster, K.F., Harris, A.I., Anderson, N. and Russell, A.P.J., 1993, ApJ 412 L67, 155-D7.
Schuster, K.F., 1994 PhD thesis, LMU Munich, Max-Planck-Inst. for ex. Phys. Report 255.
Schuster, K.F., Russell, A.P.J. and Harris, A.I., 1994, in Proc. Circumstellar Matter, Eds. Watt G.D., and Williams P.M., Kluwer Acad. Pub.
Schwarz R.D., 1990 IAU Proc. Flare Stars in Star Clusters, Associations and the Solar Vicinity, 221, L.V. Mirzoyan et al. (eds.).
Skinner S.L. and Brown, A., 1994, AJ 107 (4), 1461.
Thum C., Sievers, A., Navarro, S., Brunswig, W. and Peñalver J., 1995, IRAM Working Report No. 228/95.
van Langefelde, H.J., van Dishoek, E.F., van der Werf and Blake G.K., 1994a, ApJ 266, L94.
van Langefelde, H.J., van Dishoek, E.F. and Blake G.K., 1994b, ApJ 425, L45.
Warin, S., Benayoun, J.J. and Viala, Y.P., 1996, A&A 308, 535.
Weintraub, D.A., Masson, C.R. and Zuckerman B., 1988, ApJ 344, 915.
Witt, A.N., 1985, ApJ 294, 216.

This article was processed by the author using Springer-Verlag LaTeX A&A style file *L-AA* version 3.